TECHNIQUES AND EXAMPLES FOR THE 3D RECONSTRUCTION OF COMPLEX SCATTERING SITUATIONS USING TERRASAR-X

Nico Adam(1), Xiao Xiang Zhu(2), Christian Minet(1), Werner Liebhart(2),
Michael Eineder(1), Richard Bamler(1,2)

(1) German Aerospace Center (DLR), Remote Sensing Technology Institute (IMF), Germany
(2) Technische Universität München, Lehrstuhl für Methodik der Fernerkundung, Germany

ABSTRACT

The German radar satellite TerraSAR-X was launched in June 2007. Since then, it is continuously providing high resolution space-borne radar data which are perfectly suitable for sophisticated interferometric applications. I.e. the mission concept and the SAR sensor support the coherent stacking of radar scenes which is the basis for advanced processing techniques e.g. Persistent Scatterer Interferometry (PSI) and SAR tomography. In particular, the short repeat cycle of eleven days and the highly reproducible scene repetition of the spotlight acquisitions support the stacking and consequently the time series analysis of the radar data. Furthermore, the sensor's orbital tube is precisely controlled to be in the order of 200 m which basically allows to utilize the baseline spread of the stacked acquisitions. However, this small spread is actually limiting the resolution in the SAR tomography.
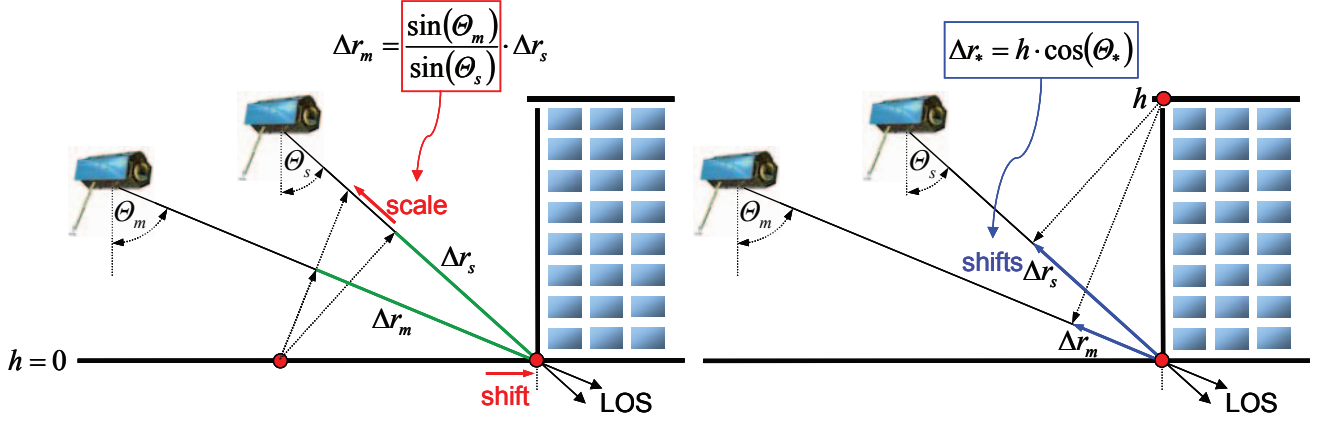
Interferometric applications could be demonstrated already in a very early stage of the TerraSAR-X mission. Because the resolution is 0.6 m in slant range and 1.1 m in azimuth in the high resolution spotlight mode the PSI and the SAR tomography processing results were impressive. Urban areas and single buildings could be mapped from space in three dimensions. Even the structural stress of single buildings caused by thermal dilation could be demonstrated. However, extended layover areas are caused by typical buildings and as a consequence complicated scattering situations need to be resolved. DLR's operational InSAR processing system GENESIS had already been adapted to cope with the new sensor modes of TerraSAR-X and their new specific spectral characteristics. Now, the new image characteristics e.g. the extended layover areas and the long time coherent distributed scatterer need better to be supported. Subject is to optimally exploit the available information e.g. the radar reflectivity. Several algorithms of the processing system can take advantage of this, e.g. the scatterer configuration detection. As a matter of fact, the scatterer configuration has now become a very important characteristic for each resolution cell. It influences e.g. the estimation data extraction, the estimation of the 3D location and basically the estimation precision. A typical resolution cell can be composed of a single dominant point scatterer surrounded by clutter, two or more dominant point scatterers in clutter and of distributed scatterers with a specific phase stability over time. The paper provides technical details and a processing example of a newly developed algorithm to retrieve the 3D location of point scatterers from the scene's intensity which finally also provides the information on the scatterer configuration in a resolution cell.

Index Terms— Persistent Scatterer Interferometry, SAR tomography, SAR radargrammetry, TerraSAR-X

1. INTRODUCTION

The SAR imaging principle is pure geometrical and related to slant range distances. As a consequence, extended layover areas are caused by typical buildings making the interpretation of radar images in urban areas difficult. Essentially, the problem is that scatterers on the ground and on the building are mapped into one and the same resolution cell. This ambiguity can not be resolved with a single radar acquisition. Practical solutions of this problem are SAR tomography [1], [2], [3] which retrieves the radar reflectivity in cross slant range and the persistent scatterer interferometry (PSI) [4], [5] which estimates the height and displacement of the point scatterers. Both are coherent (i.e. phase based) methods working on a stack of scenes acquired with different look angles. However, this causes some limitations in the application of this technique. Difficulties are caused e.g. by the temporal decorrelation and a small spread of look angles. The first reduces the number of available acquisitions. The latter limits the PSI height estimation precision and the spatial resolution in cross slant range for SAR tomography. The small spread of look angles results from the controlled small orbital tube of the sensor TerraSAR-X providing a standard deviation of 100 m for the effective baselines. Other challenges in the retrieval result from the atmospheric phase screen (APS) and the displacement because both alter the phase. Unfortunately, the displacement can even be non-linear and a displacement

Fig 1: geometrical effects of the coregistration (left figure) and the height of a scatterer (right figure).

model selection needs to be included into the estimation process. Of course, the number of models which can be tested is practically limited. Ideally, the scatterer location should be available beforehand in order to predict complicated scattering situations (e.g. layover, shadow) and to separate their detection or the model order selection from the estimation. Of course, this requires precise DEM information which is usually not available. A solution is to derive this information directly from the data using an alternative method which is not sensitive to temporal decorrelation, APS and displacement. A suitable technique is an amplitude based algorithm similar to radargrammetry [6], [7]. Unfortunately, the look angle spread in a typical interferometric stack (i.e. a single beam) is too small to practically measure the height of typical buildings from the induced scatterer shift. This is the reason scenes acquired from different beams are used in the implemented procedure.

2. ESTIMATION PRINCPLE

The implemented procedure is radargrammetric and consequently it is only based on the radar amplitude. In principle, the change of the slant range distance caused by varying look angles is utilized. I.e. scatterers with different heights are mapped into different range locations of the SAR scene. The scatterer's slant range offset can be measured very precisely and unambiguously due to the large look angle range of 20-55 degree and the high spatial resolution of ca. 0.5 m of the sensor TerraSAR-X. In fact, the wide look angle range is achieved by the combination of acquisitions taken with different beams. Such scenes can easily be ordered because the sensor TerraSAR-X offers this flexibility operationally.

The newly developed radargrammetry method further gains precision by the following two features. Firstly, the estimation is restricted to point scatterers only. And secondly, several scenes per beam i.e. with a similar look angle are used. The first detail allows combining scenes with a large look angle spread and collected over a long time span

due to the point scatterers radiometric stability. This is the reason the used points are called radiometric persistent scatterer (RPS). The second feature results in a reduction of speckle. I.e. weak scatterers can better be detected which could result from the look angle dependent impulse response.

Essentially, two effects in range direction need to be considered by the algorithm. On the one hand the coregistration and on the other the height of the RPS acts. The coregistration provides the alignment of all scenes regarding a master scene. More precisely, the resolution cells on the ground with zero height (i.e. $h = 0$) are aligned in the stack of acquisitions. In the range direction this is achieved in principle by shifting and scaling the slave images. The scaling corrects for the look angle (i.e. Θ_m for master and Θ_s for slave look angle) dependent range resolution of the acquisitions. As a result the slant range distances Δr_m in the master scene and Δr_s in the slave scenes correspond to the same distance on the ground, i.e.

$$\Delta r_m = \frac{\sin(\Theta_m)}{\sin(\Theta_s)} \cdot \Delta r_s \qquad (1)$$
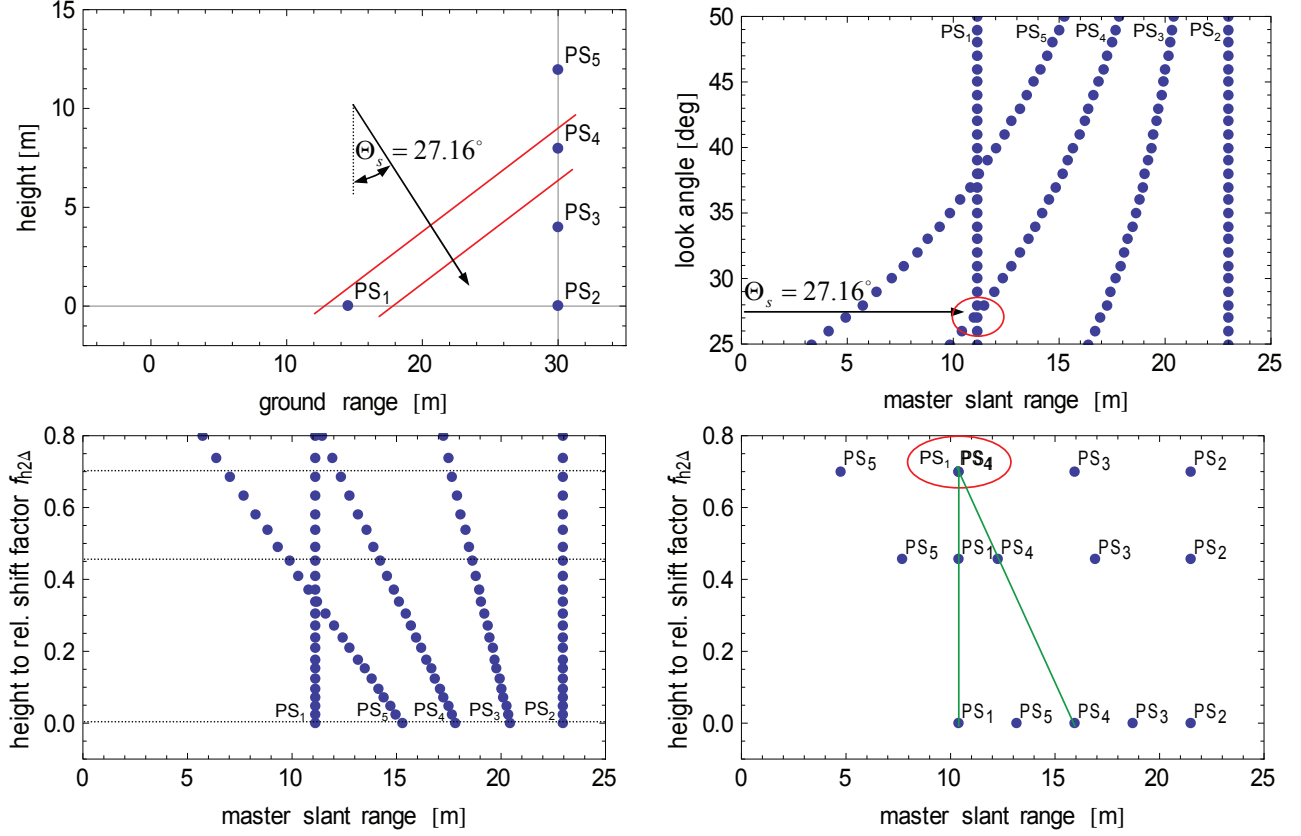
This principle is visualized in Fig.1 on the left hand side. Additionally, the local height of a RPS introduces another look angle dependent shift Δr_m for the master scene and Δr_s for the slave scenes:

$$\Delta r_m = \cos(\Theta_m) \cdot h \quad \text{and} \quad \Delta r_s = \cos(\Theta_s) \cdot h \qquad (2)$$

This principle is visualized in Fig.1 on the right hand side. Both range shifts take effect at the same time. In other words, the zero height related coregistration also influences the RPSs with a height h and consequently a relative shift Δ of the RPSs related to the master scene can be measured:

$$\Delta = \left(\frac{\sin(\Theta_m - \Theta_s)}{\sin(\Theta_s)} \right) \cdot h = f_{h2\Delta} \cdot h \qquad (3)$$

It is worth noticing, the relative shift Δ (in units of meter) is linear dependent on the height h of a RPS. This linearity is

Fig. 2: illustration of the measurements for a typical scatterer configuration (details are in section 2).

described by the *height to relative shift factor* $f_{h2\Delta}$ and corresponds to the term put in parentheses in equation 3. The factor is computed by a non-linear re-scaling of the actual look angle Θ_s of the current slave scene related to the look angle Θ_m of the master scene. The acquisition with the largest look angle should be selected as the master scene. As a result, the coregistration stretches all slave scenes.

Practically, at least three different beams i.e. significant different look angles are required. The reason is that RPSs can be located on the same range line and close together. In this situation the association of one and the same RPS in the different scenes to each other is ambiguous with two angles only. The situation improves with three look angles and gets even better with more acquisitions (i.e. look angles). The principle of the association of one and the same RPS to each other in the different acquisitions and the height estimation is visualized in Fig.2 using a synthetic example. The top left image shows a typical scatterer configuration with RPSs on ground (index 1 and 2) and some RPSs on a vertical wall (indices 2-5). In the top right image, the RPS's mapping into the master slant range geometry is visualized depending on the look angle. Obviously, this mapping depends on the height and is non-linear. In the bottom left plot, the linearized relation of the RPS shift related to the *height to rela-*
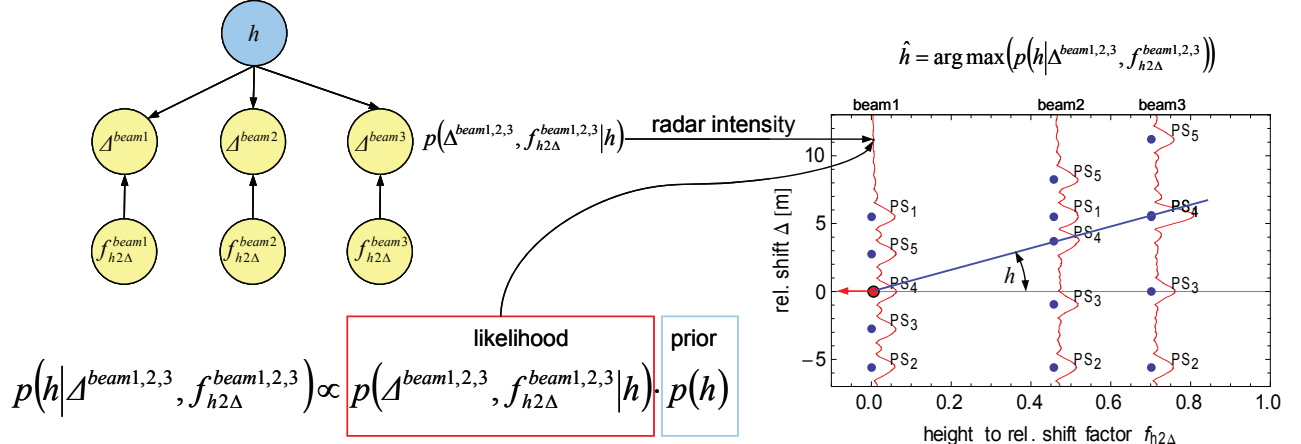
tive shift factor $f_{h2\Delta}$ by rescaling of the look angles is shown. The latter plot also shows that the RPSs can be unambiguously assigned to each other easily in case many observations from different look angles are available. However, typically only few look angles are available and in the lower right figure this situation is visualized for three available look angles of 27.16, 31.86 and 45.85 deg. The corresponding scatterers are assigned by a line fit which always starts from the detected RPS in the master scene. A usable RPS is found in case a RPS is on the fitted line in each scene. Finally, the slope of the line corresponds to the estimated absolute height.

3. IMPLEMENTATION DETAILS

The practically implemented framework is based on Bayesian inference using directed graphs and maximizes the posterior probability of the estimated height $\hat{h}$ given the likelihood of the offset measurements $p\left(\Delta^{beam1,2,3}\right)$:

$$\hat{h} = \arg\max\left(p\left(h\middle|\Delta^{beam1,2,3}, f_{h2\Delta}^{beam1,2,3}\right)\right) \qquad (4)$$

(with $\Delta^{beam1,2,3} \triangleq \Delta^{beam1}, \Delta^{beam2}, \Delta^{beam3}$ and with $f_{h2\Delta}^{beam1,2,3} \triangleq f_{h2\Delta}^{beam1}, f_{h2\Delta}^{beam2}, f_{h2\Delta}^{beam3}$). We take the intensity along the range line as the likelihood for a certain RPS offset. In doing this,

$$\hat{h} = \arg\max\left(p\left(h\left|\Delta^{beam1,2,3}, f_{h2\Delta}^{beam1,2,3}\right.\right)\right)$$

$$p\left(h\left|\Delta^{beam1,2,3}, f_{h2\Delta}^{beam1,2,3}\right.\right) \propto \underbrace{p\left(\Delta^{beam1,2,3}, f_{h2\Delta}^{beam1,2,3}\left|h\right.\right)}_{\text{likelihood}} \cdot \underbrace{p(h)}_{\text{prior}}$$

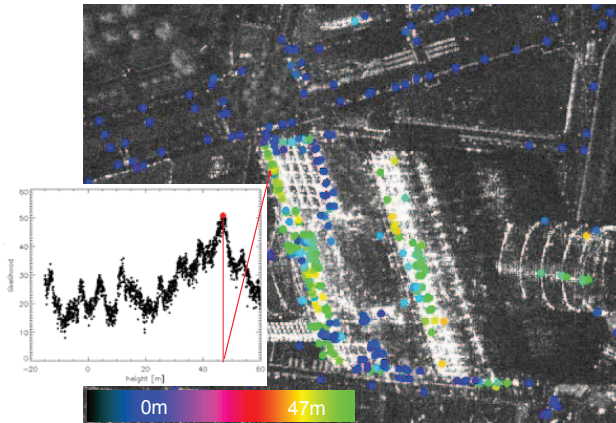**Fig.3:** dependency graph of the observations (left figure) and the corresponding estimation principle (right figure).

the directed graph allows the inference from the likelihood and the prior $p(h)$:

$$p\left(h\left|\Delta^{beam1,2,3}, f_{h2\Delta}^{beam1,2,3}\right.\right) \propto p\left(\Delta^{beam1,2,3}, f_{h2\Delta}^{beam1,2,3}\left|h\right.\right) \cdot p(h) \quad (5)$$

The framework can easily handle multi modal likelihood functions and consequently complicated scattering situations. Again, the estimation is a simple Bayesian line fitting with multi modal pdfs and the dependency graph is shown in Fig.3. The estimation can benefit from a joined estimation of a small neighborhood. The Bayesian framework allows to test for the hypotheses of a vertical wall and a horizontal surface.

4. APPLICATION TEST CASE

The Berlin's central station is selected as a test site. Fig.4 provides a preliminary estimation of the building's height. Many points on this building can finally be used for this estimation principle. The inserted image on the left of Fig.4 provides the likelihood of the height for the highlighted point. In this example only a single dominant peak can be detected. In case of a resolution cell with more scatterers the according number of pronounced peaks at the specific

Fig. 4: preliminary estimation of the building's height.

height can be found. The width of the single peak provides the information on the height estimation precision.

5. SUMMARY

A new algorithm using detected radar images only to support PSI and SAR tomography has been developed. It provides the 3D scatterer location and the resolution cell configuration. Advantageously, it is not limited by the sensor's small orbital tube, temporal decorrelation, APS and the scatterer's displacement. The proposed technique will take profit of future SAR systems with 600 MHz bandwidth.

6. ACKNOWLEDGEMENT

We would like to thank Thomas Fritz, Kanika Goel and the TMSP team headed by Helko Breit for their support.

7. REFERENCES

[1] Fornaro G., Monti Guarnieri C., Pauciullo A. and S. Tebaldini, "Joint multi-baseline SAR interferometry," *EURASIP J. Appl. Signal Process*, vol. 20, pp. 3194–3205, 2005.

[2] Reigber A. and Moreira, A., "First demonstration of airborne SAR tomography using multibaseline L-band data", *TGARS*, vol. 38, no. 5, pp. 2142-2152, 2000.

[3] Zhu X., Adam N. and R. Bamler, "Space-borne High Resolution SAR Tomography: Experiments in Urban Environment Using TS-X Data", *Proc. of Joint Urban 2009*, Shanghai, 2009.

[4] Ferretti A., C. Prati and F. Rocca, "Permanent Scatterers in SAR Interferometry", *TGARS*, Vol. 39, No. 1, pp. 8-20, 2001.

[5] Adam N., Bamler R., Eineder M. and B. Kampes, "Parametric estimation and model selection based on amplitude-only data in PS-interferometry", *Proc. of FRINGE'05*, Frascati, on CD, 2005.

[6] Bamler, Richard, "Interferometric Stereo Radargrammetry: Absolute Height Determination from ERS-ENVISAT Interferograms", *Proc. of IGARSS 20000*; Hawaii, on CD, 2000.

[7] Bamler, R, M. Eineder, "Accuracy of Differential Shift Estimation by Correlation and Split Bandwidth Interferometry for Wideband and Delta-k SAR Systems", *GRSL*, vol. 2, pp.151-155, 2005.